Journal of Solid State Chemistry **160,** 394–400 (2001)
doi:10.1006/jssc.2001.9253, available online at http://www.idealibrary.com on IDEAL®

Floating Zone Crystal Growth and Structure Analysis of a Novel ScB_{19} Family Compound, $ScB_{19+x}Si_y$

Takaho Tanaka[1] and Akira Sato

Advanced Materials Laboratory, National Institute for Materials Science, Namiki 1-1, Tsukuba, Ibaraki 305-0044, Japan

Received February 9, 2001; in revised form May 10, 2001; accepted May 25, 2001; published online July 23, 2001

Single crystals of a novel ScB_{19} family compound $ScB_{19+x}Si_y$ were grown by the floating zone method using a four-lamp mirror-type image furnace. A small amount of silicon addition to ScB_{19} which decomposes at elevated temperatures without melting allowed it to coexist with the liquid phase and as a resultant made the floating zone crystal growth possible. Powder X-ray diffraction analysis confirmed the grown crystals of $ScB_{19+x}Si_y$ to be isostructural to ScB_{19}. It was found that the crystal structure of $ScB_{19+x}Si_y$ solved based on single-crystal X-ray data is tetragonal with lattice constants of a, $b = 1.03081(2)$ nm, $c = 1.42589(3)$ nm, space group $P4_12_12$ or $P4_32_12$ and is basically isotypic with α-AlB_{12} structure type. In the crystal structure boron atoms form a three-dimensional framework based on interconnected B_{12} icosahedra and B_{22} polyhedra. The Sc atoms reside in three of five Al sites in the α-AlB_{12} structure and Si resides in a bridge site bonding two B_{22} units.

Key Words: **boron-rich scandium boride; scandium borosilicide; floating zone crystal growth; $ScB_{19+x}Si_y$; ScB_{19}; tetragonal crystal structure; icosahedral boron cluster.**

1. INTRODUCTION

After a YB_{66} soft X-ray monochromator was first installed on BL3-3 of Stanford Synchrotron Radiation Laboratory in early 1993 (1) and became practical, its use has gradually spread on soft X-ray beamlines of worldwide synchrotron radiation facilities. However, amorphous-like low thermal conductivity of YB_{66} restricts its installation only on beamlines having rather low beam intensities. It is not so easy to remove heat locally generated by irradiation with a brighter X-ray beam coming from an undulator or wiggler, and as a result the resolution of the YB_{66} monochromator would be reduced.

One of the authors (T.T.) has continuously searched for new boron-rich compounds which can replace YB_{66} by not only satisfying requirements as a soft X-ray monochromator material but also having higher thermal conductivity than YB_{66}. The effort has born many novel rare-earth(RE) boron-rich borides like REB_{25} (2), REB_{50} (3), ScB_{19} (4), $ScB_{17}C_{0.25}$ (5), and so on (6). However, all these compounds decompose at elevated temperatures without melting so that it is impossible to apply the melt growth method to these compounds. Single crystals of most boron-rich compounds have been grown by the high-temperature solution growth method using metal fluxes like Al, Cu, Sn, and so on; however, the method can give only millimeter-size crystals which are not useful for the monochromator application.

An exceptional example is crystal growth of the REB_{50} phase. The author found that a small amount of Si addition to REB_{50} allowed it to coexist with the liquid phase without decomposing, which as a resultant made the floating zone crystal growth of REB_{50} possible. In fact, single crystals of ternary $YB_{41}Si_{1.2}$ which is isotypic with YB_{50} have been grown by applying the Si addition method (7). Single-crystal structure analysis revealed that the orthorhombic crystal structure of $YB_{41}Si_{1.2}$ is a completely new structure type of boron-rich borides (8). However, the obtained single crystals included some cracks; thus, we quit our efforts to obtain monochromator-grade quality single crystals.

ScB_{19}, whose crystal structure is tetragonal (lattice constant a, $b = 1.02915(4)$ nm, and $c = 1.42463(9)$ nm, and expected space group $P4_12_12$ or $P4_32_12$, is a newly found binary compound (4) and is expected to be isotypic to α-AlB_{12} because of similarities in cell dimensions and space groups (9). Lack of single crystals has prevented proving it. In order to obtain single crystals for structure analysis and to secure footing for a new monochromator material, the Si addition method was applied to ScB_{19} as the second example.

In the present paper the floating zone crystal growth of the Si-added ScB_{19} and single-crystal structure analysis are presented.

[1]To whom correspondence should be addressed. E-mail: TANAKA.Takaho@nims.go.jp.

0022-4596/01 $35.00

2. EXPERIMENTAL

2.1. Floating Zone Method

Raw powders of ScB_{19} were synthesized by a boro-thermal reduction method using powders of Sc_2O_3 (3N, Crystal Systems Inc., Japan) and amorphous boron (3N, SB-Boron Inc., USA). Details of the powder synthesis of ScB_{19} are given elsewhere (4). After addition of a suitable amount of silicon, the powder was pressed into a green rod by the CIP (cold isostatic press) process at 250 MPa. The green rod was sintered in a boron nitride crucible at about 1700°C for several hours in vacuum. Because of the strong covalent character of boron-rich borides, no shrinkage could be expected during the sintering process and the density of the sintered rods stayed at about 60% of the theoretical value. The $ScB_{19}Si_y$ phase incongruently melts and coexists with a silicon-rich liquid. Thus the composition of the molten zone should be much richer in silicon. However, infiltration of such a silicon-rich melt into the porus sintered rod could happen very easily and a silicon less-rich melt remained at the molten zone, causing a growth of mixed phases of ScB_{12} and Sc-doped β-boron. In order to avoid this trouble by achieving nearly 100% theoretical density of the feed rod, horizontal zone-melting of the sintered rod was applied to the sintered rods on a boron nitride half-cut pipe crucible by a horizontal zone-melting image furnace.

The floating zone crystal growth was carried out using a four-ellipsoid mirror-type image furnace (Crystal Systems Inc., Japan) which is expected to have a smaller temperature gradient around the crystal radius than a single mirror- or double mirror-type image furnace. The feed rod and the seed rod were set on the upper and lower axes, respectively. A pellet whose composition is expected to be coincident with that of the molten zone was put on the top of the seed rod. When the pellet started melting, the molten zone was formed by touching the bottom of the feed rod to the melt. The floating zone crystal growth then started by downward driving of both the feed rod and the seed rod synchronously at a rate of 5–7 mm/h. Both rods were counter-rotated at ± 35 rpm and the atmosphere was flowing Ar.

2.2. Chemical Analysis

The chemical compositions of several parts of the crystals were determined by complete wet chemical analysis. After the crystal was crushed to a powder in a stainless-steel mortar and the stainless-steel contamination was washed by a dilute HCl solution and rinsed away, the obtained powder was dissolved in a HNO_3/HCl (1:1) solution, keeping it at 150°C for 16 hours in an air-tight capsule, and the scandium, boron, and silicon contents were determined by inductively coupled plasma atomic emission spectroscopy.

TABLE 1
Crystal and Intensity Measurement Data

Crystal composition	$ScB_{19.2}Si_{0.25}$[a]
Crystal system	Tetragonal
Space group	$P4_32_12$
a, c (nm)	1.03081(2), 1.42589(3)
V (nm^3)	1.51511(5)
Structural formula (chemical composition[b])	$Sc_{2.26} \cdot 2B_{12} \cdot B_{20.6} \cdot Si_{0.41}$ $(ScB_{19.7}Si_{0.18})$
D_x (g/cm^3)	2.610
D_m (g/cm^3)	2.635
Z	4
μ for Mo$K\alpha$ (cm^{-1})	10.43
Crystal dimensions (mm)	$0.35 \times 0.35 \times 0.25$
Reflection measured	$0 \le h \le 16$, $0 \le k \le 16$, $0 \le l \le 23$
$2\theta_{max}$	70 deg
NR[c]	1965
NV[d]	131

[a]Obtained by chemical analysis. [b]Obtained by structure analysis. [c]Number of independent reflections. [d]Number of variable parameters.

2.3. X-Ray Diffraction

Phase identification was carried out using a standard powder X-ray diffractometer (R-2000, Rigaku Co., Japan) with Cu$K\alpha$ radiation and the same powder was used in chemical analysis. The X-ray single-crystal data were collected on an Enraf-Nonius CAD4 automatic four-circle diffractometer with graphite-monochromated Mo$K\alpha$ radiation. The intensity data were corrected for Lorentz and polarization effects. The crystallographic data and intensity measurement data are given in Table 1. The absorption correction applied to the collected data was empirical based on Ψ-scans.

3. RESULTS AND DISCUSSION

3.1. Crystal Growth

The binary Sc–B phase diagram is given in Fig. 1 where ScB_{19} is added to the previously reported phase diagram (10). The ScB_{19} phase decomposes into ScB_{12} and β-boron at 1850°C without melting. Thus, the melt growth of ScB_{19} single crystal is impossible; however, the decomposition temperature is only 100°C below the eutectic temperature. Si addition which can reduce the melting temperature of borides may allow ScB_{19} to melt before its decomposition, similar to the case with the YB_{50} phase. In order to test the effect of Si addition on ScB_{19} a sample with composition $ScB_{19} + 3Si$ was arc-melted. The powder XRD analysis of the arc-melted sample showed the existence of the ScB_{19} phase which survived without decomposing after the arc-melting experiment. This fact proved that the melt growth method can be applied to the Si-doped ScB_{19} single-crystal growth.

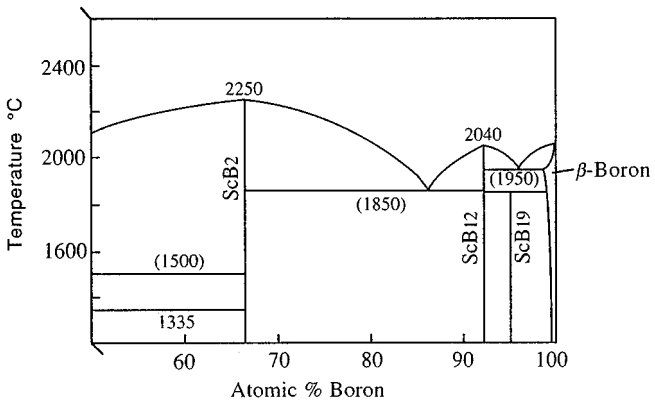

FIG. 1. The binary Sc–B phase diagram.

Several itinerant experiments could not give reproducible Si contents in the feed rods. This seemed to be due to low quality of Si powder which was fairly oxidized. SiB_6 was then used as a silicon source. For example, at first $ScB_{17.5}$ was synthesized and then SiB_6 was reacted with $ScB_{17.5}$ according to the following reaction equation, $ScB_{17.5} + 0.4SiB_6 = ScB_{19.9}Si_{0.4}$.

After 4 times horizontal zone-melting through the sintered rod of $ScB_{19.9}Si_{0.4}$ thus obtained, the rod density became nearly 100% and the rod had an ellipsoidal cross section. Floating zone crystal growth was carried out using the zone-melted rod.

Figure 2 shows an example of a grown crystal whose dimensions are about 8 mm in diameter and 50 mm in length. Many irregular ridges which probably correspond to grain boundaries can be seen on the crystal surface even after a more than 40 mm zone pass. It seems not so easy to obtain a single-grain crystal. It was confirmed that the grown Si-doped crystal and ScB_{19} are isostructural by comparing their powder XRD patterns as shown in Fig. 3, where several extra peaks marked by an arrow in the XRD patterns of ScB_{19} are due to residual ScB_{27} (Sc-doped β-boron). Hereafter, $ScB_{19+x}Si_y$ is used to refer to the Si-doped ScB_{19}, because the composition is variably dependent on the experimental crystal growth conditions.

Compositions of the crystal shown in Fig. 2 are summarized in Table 2. The composition of the feed rod is rather Sc rich as compared with the first raw composition set at $ScB_{19.9}Si_{0.4}$. B and Si must be lost more than Sc during the repeated horizontal zone melting. The Sc/B ratio in the molten zone is close to ScB_{12}. The eutectic composition between ScB_{12} and ScB_{27} (Sc-doped β-boron) in the binary Sc–B system is expected to be about B/Sc = 20 as shown in Fig. 1. The ternary eutectic composition shifts toward the Sc-rich side by Si addition. The fact that the Si content in the crystal is higher than that in the feed rod contradicts the fact that Si evaporates faster than Sc and B. Probably the Si content in the initial molten zone was too high and was gradually distributed into the crystal, which is consistent with the fact that the Si content in the zone-end crystal is lower than those of others and comes closer to that of the feed rod.

The Si partition coefficient at the growth interface which is the ratio of the Si contents in the zone-end crystal and in the molten zone is about 0.1. Because of large composition differences for both boron and silicon between the molten zone and the growing crystal, the Si-doped ScB_{19} crystal growth is closer to the high-temperature solution growth than the melt growth.

3.2. Structure Analysis

A single-crystal specimen for four-circle XRD data collection was obtained by cracking a part of one of the floating zone grown crystals and the remaining part was sent for chemical analysis which gave a composition of $ScB_{19.2}Si_{0.25}$.

Without using the α-AlB_{12} structure model, an initial structure solution was obtained by SIR92 (11) and the program SHELXL-97 (12) was used for refinement, where space group $P4_32_12$ was adopted for easier comparison with the previous result of α-AlB_{12}. The direct method gave 28 atomic positions in which one Sc, one Si, and 26 B were assigned. Comparison between the obtained atomic coordinates and those of α-AlB_{12} showed immediately that they are isotypic. Based on the α-AlB_{12} site assignment two B sites whose coordinates are coincident with those of Al sites were reassigned to Sc sites. One of two new B sites was reassigned to a Si site. On the other hand, the site first assigned as a Si site coincided with a B(18) site of α-AlB_{12} and was reassigned as a B site. Thus, three Sc sites, one Si site, and 24 B sites were finally assigned. A final refinement

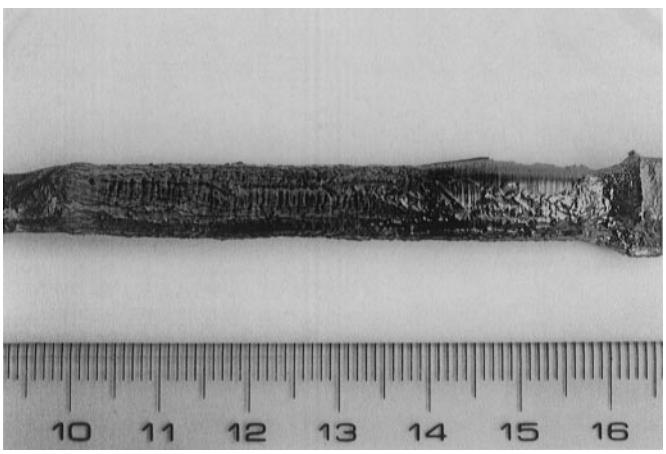

FIG. 2. A single crystal of $ScB_{19+x}Si_y$ grown by the floating zone method.

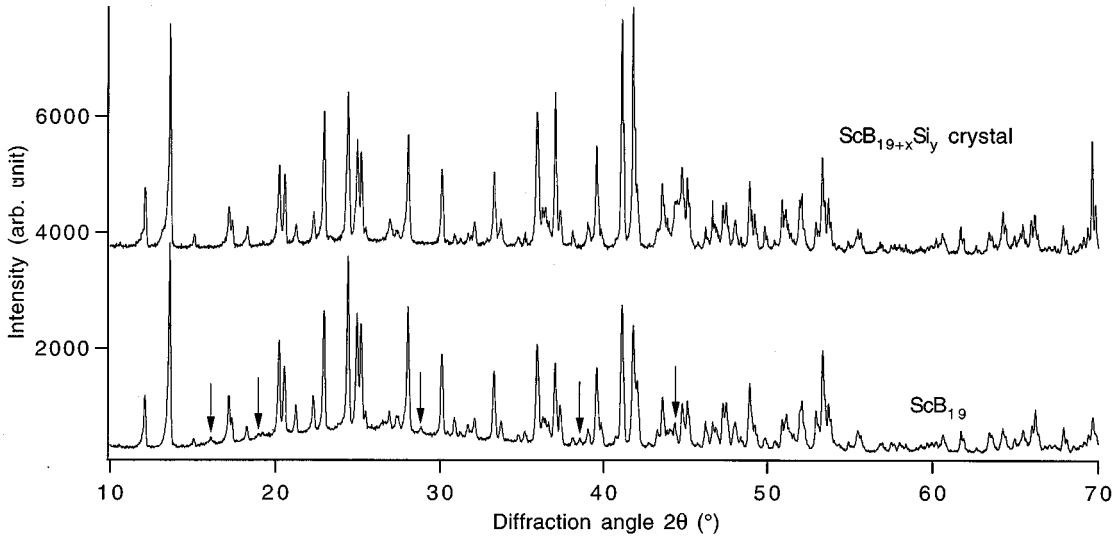

FIG. 3. Comparison of powder XRD patterns of ScB_{19} and $ScB_{19+x}Si_y$ crystal. Several extra peaks marked by an arrow in the ScB_{19} XRD pattern are due to residual ScB_{27} (Sc-doped β-boron).

of 131 parameters for 1965 independent reflections resulted in an $R1$ value of 3.1% and a w$R2$ value of 8.2%.

The resultant atomic positions and the occupancies of the partially occupied sites are listed in Table 3 and the interatomic distances are listed in Table 4. Although $ScB_{19+x}Si_y$ is isotypic to α-AlB_{12}, there are several differences between them. The crystal structure of α-AlB_{12} is characterized by a boron framework structure consisting of B_{12} icosahedra and B_{19} units where a B_{19} unit is a twinned icosahedron with two vacant sites (9). A new boron site B(24) was found to coincide with the vacant sites. Most boron sites are fully occupied similar to α-AlB_{12}, but the B(18) and B(24) sites are partially occupied with occupancies of 65.2 and 63.1%, respectively. Both sites are too close to Si and Sc(2) sites, respectively, so that simultaneous occupation at the neighboring sites of B(18)–Si or B(24)–Sc(2) cannot happen. The Si site is also too close to both Sc(2) and Sc(3) sites and their site occupancies are only 20.3, 19.4, and 12.8%, respectively. Three Sc sites, Sc(1), Sc(2), and Sc(3), correspond to the Al(4), Al(1), and Al(2) sites of α-AlB_{12}, respectively. The Al(3) and Al(5) sites are empty for $ScB_{19+x}Si_y$.

TABLE 2
Chemical Composition of the Grown Crystal Shown in Fig. 2

Position	Composition
Feed rod	$ScB_{17.8}Si_{0.17}$
Zone	$ScB_{12.4}Si_{1.90}$
Zone-end part crystal	$ScB_{18.0}Si_{0.22}$
Middle part crystal	$ScB_{19.2}Si_{0.27}$
Initial part crystal	$ScB_{19.0}Si_{0.27}$

The chemical composition $ScB_{19.7}Si_{0.18}$ obtained from the structure analysis is in good agreement with that ($ScB_{19.2}Si_{0.25}$) obtained from chemical analysis. The X-ray density of 2.610 g/cm^3 agrees with the measured density of 2.635 g/cm^3.

The boron framework of $ScB_{19+x}Si_y$ crystal structure is made up by one B_{12} icosahedron and one B_{22} unit which can be observed in β-tetragonal boron (13) and is a modification of the B_{20} unit of α-AlB_{12} (14) or the B_{19} unit in the earlier paper (9). The B_{20} unit is a twinned icosahedron made up of B(13) to B(22) with two vacant sites and one B atom (B(23)) bridging both sides of the unit. B(23) was treated as an isolated atom in the earlier discussion of the α-AlB_{12} crystal structure (9). B(23) is bonded to each of the twinned icosahedra through B(18) and another icosahedron through B(5). If the twinned icosahedra were independent without twinning, B(23) would be really a bridge site which links three icosahedra. However, because of twinning B(23) bonds closer to the twinned icosahedra than another icosahedron; recently B(23) was treated as a member of the twinned icosahedra. In the case of $ScB_{19+x}Si_y$, the two B(24) sites which correspond to the vacant sites in the B_{20} unit are partially occupied as noted above; thus, the unit should be referred to as the B_{22} unit which is occupied by about 20.6 boron atoms.

On the other hand, Si is bonded to B(23) and B(24) of one B_{22} unit and B(13) of another B_{22} unit. The Si–B(13) bond distance is much shorter than those of Si–B(23) and Si–B(24) and the Si site can be understood as a bridge site linking two B_{22} units. The arrangement of the B_{22} unit and

TABLE 3
Final Atomic Coordinates, Temperature Factors, and Occupancy Factors

Atom	Site	x	y	z	$U(\text{Å}^2 \times 10^3)$	Atom	Site	x	y	z	$U(\text{Å}^2 \times 10^3)$
B(1)	8(*b*)	−0.1228	0.2389	0.1261	5.06	B(15)	8(*b*)	0.2135	0.1978	0.3449	10.19
B(2)	8(*b*)	−0.0333	0.1355	0.2097	5.50	B(16)	8(*b*)	0.4700	0.1142	0.4131	6.57
B(3)	8(*b*)	−0.0428	0.3116	0.2294	5.18	B(17)	8(*b*)	0.4662	0.2887	0.4239	6.27
B(4)	8(*b*)	−0.0398	0.3917	0.1159	5.36	B(18)	8(*b*)	0.1903	0.0946	0.4509	9.15
B(5)	8(*b*)	−0.0113	0.1129	0.0786	6.27	B(19)	8(*b*)	0.2721	0.1861	0.5453	6.32
B(6)	8(*b*)	−0.0273	0.2720	0.0277	5.24	B(20)	8(*b*)	0.3529	0.0420	0.4933	6.37
B(7)	8(*b*)	0.1154	0.2258	0.2440	5.93	B(21)	8(*b*)	0.4445	0.1865	0.5260	8.90
B(8)	8(*b*)	0.1027	0.3902	0.1920	5.46	B(22)	4(*a*)	0.3354	0.3354	0.5000	8.92
B(9)	8(*b*)	0.1265	0.1058	0.1548	5.73	B(23)	4(*a*)	0.0347	0.0347	0.5000	10.25
B(10)	8(*b*)	0.1270	0.1951	0.0453	5.04	B(24)	8(*b*)	0.3133	0.3367	0.3810	14.73
B(11)	8(*b*)	0.1142	0.3624	0.0645	5.16	Sc(1)	8(*b*)	0.2964	0.4857	0.1316	4.73[a]
B(12)	8(*b*)	0.2093	0.2618	0.1403	5.22	Sc(2)	8(*b*)	0.2981	0.3750	0.2968	16.22[a]
B(13)	8(*b*)	0.3187	0.0588	0.3634	9.81	Sc(3)	8(*b*)	0.0849	0.0107	0.3215	5.66[a]
B(14)	8(*b*)	0.3933	0.2069	0.3260	8.95	Si	8(*b*)	0.1758	0.0037	0.4227	10.09

Atom	U_{11}	U_{22}	U_{33}	U_{12}	U_{13}	U_{23}
Sc(1)	4.74	4.64	4.81	0.68	0.33	0.44
Sc(2)	9.50	7.69	31.47	4.20	4.40	3.59
Sc(3)	4.81	5.71	6.45	1.71	0.20	0.68

Occupancy factors of the partially occupied sites
B(18): 65.2% B(24): 63.1% Sc(1): 81.1% Sc(2): 19.4% Sc(3): 12.8% Si: 20.3%

[a]For Sc sites anisotropic thermal factors are applied and U_{eq} is noted in these columns.

Si is shown in Fig. 4. If a Si site occupancy of 20.3% is taking into consideration, only five Si atoms can be accommodated on the 12 Si sites in the unit cell.

The intraicosahedral and intericosahedral B–B bond distances range from 1.725(3) to 1.897(2) and from 1.630(3) to 1.883(4) Å, respectively. The mean value of the intraicosahedral B–B bond distance 1.813 Å agrees well with values of 1.805 Å for α-AlB_{12} and 1.810 Å for AlB_{10} (15); however, the variation in the B–B bond distances is more significant as compared with those observed in both α-AlB_{12} (1.736–1.858 Å) and AlB_{10} (1.783–1.839 Å). The mean value of the intericosahedral B–B bond distance, 1.749 Å, is larger than the value of 1.709 Å for both α-AlB_{12} and AlB_{10}. The larger ionic radius of Sc than Al elongated the intericosahedral bonds without changing the size of icosahedron. The angles of the triangles of the icosahedron range from 57.0(1)–63.3(1)°. The variation in the angles is not so different from that observed in α-AlB_{12} (57.0(1)–62.0(1)°) as compared with the difference observed in the bond distances.

The bond lengths in a B_{22} unit range from 1.755(3) to 1.939(2) Å with a mean value of 1.821 Å, except for one unusual length of 1.977(6) Å between B(18)–B(18) atoms which belong to a different side of B_{22} twinned icosahedra. The mean value is also larger than that of α-AlB_{12} (1.814 Å). The angles of the triangles of the B_{22} unit vary from 57.1(1)–65.3(1)°.

The B–B length bonding B_{22} units is 1.716(3) Å which is almost same as that (1.715(3) Å) bonding B_{20} units in α-AlB_{12}. The lengths of the bonds directly connecting the B_{12} and B_{22} units range from 1.671(3) to 1.873(3) Å with a mean value of 1.747 Å. The B_{12} and B_{22} units are also connected through the B(5)–B(23) bond with a rather large bond length of 1.906 Å.

The Sc(1) site which corresponds to the Al(4) site (15.0% site occupancy) of α-AlB_{12} has a characteristically high site occupancy of 81.1% and the Sc(2) and Sc(3) sites which correspond to the Al(1) and Al(2) sites (71.7 and 49.1% site occupancies, respectively) have much lower site occupancies of 19.4 and 12.8%, respectively. The shortest distance between Sc and B of the Sc(1) site (2.298 Å) is fairly longer than those (2.035 and 2.185 Å, respectively) of the other two sites. Probably the larger diameter of Sc prefers a larger volume of the Sc(1) site as compared with the case of Al in α-AlB_{12}. Along this consideration one may expect a higher site occupancy of the Sc(3) site than the Sc(2) site, however, the Sc(3) site is separated by only 2.395(3) Å from a neighbor Sc(1) site and 2.470(5) Å from another Sc(3) site. In rare-earth boron-rich borides rare-earth atoms are expected to be trivalent ions donating their valence electrons to the boron lattice bonding so that simultaneous occupancy of those sites can hardly occur, and as a result the site occupancy of the Sc(3) site becomes low. Even for the Sc(2) sites which are separated by only 2.617(2) Å from the Sc(1) site

TABLE 4
Interatomic Distances (Å)

B–B Bond Length within B_{12} Icosahedron							
B(1)–B(2)	1.846(3)	B(2)–B(9)	1.849(3)	B(5)–B(9)	1.790(3)	B(8)–B(11)	1.843(2)
–B(3)	1.847(2)	B(3)–B(4)	1.816(2)	–B(10)	1.725(3)	–B(12)	1.871(3)
–B(4)	1.799(3)	–B(7)	1.867(3)	B(6)–B(10)	1.795(3)	B(9)–B(10)	1.813(2)
–B(5)	1.861(3)	–B(8)	1.787(3)	–B(11)	1.809(3)	–B(12)	1.832(3)
–B(6)	1.747(2)	B(4)–B(6)	1.767(3)	B(7)–B(8)	1.854(3)	B(10)–B(11)	1.751(3)
B(2)–B(3)	1.839(3)	–B(8)	1.826(3)	–B(9)	1.778(3)	–B(12)	1.739(2)
–B(5)	1.897(2)	–B(11)	1.774(3)	–B(12)	1.806(2)	B(11)–B(12)	1.789(3)
–B(7)	1.858(3)	B(5)–B(6)	1.801(3)				
B–B Bond Lengths Within B_{22} Unit							
B(13)–B(14)	1.791(3)	B(14)–B(24)	1.757(4)	B(17)–B(22)	1.796(2)	B(19)–B(20)	1.857(3)
–B(15)	1.817(3)	B(15)–B(18)	1.863(4)	–B(24)	1.762(4)	–B(21)	1.799(3)
–B(16)	1.805(3)	–B(19)	1.765(3)	B(18)–B(18)	1.977(6)	–B(22)	1.792(3)
–B(18)	1.856(4)	–B(24)	1.837(4)	–B(19)	1.831(4)	–B(24)	1.807(4)
–B(20)	1.893(3)	B(16)–B(17)	1.805(3)	–B(19)	1.847(4)	B(20)–B(21)	1.825(3)
B(14)–B(15)	1.876(3)	–B(20)	1.822(3)	–B(20)	1.863(4)	B(21)–B(22)	1.939(2)
–B(16)	1.755(3)	–B(21)	1.793(3)	–B(23)	1.856(4)		
–B(17)	1.797(3)	B(17)–B(21)	1.810(3)	B(19)–B(19)	1.800(4)		
B–B Bond Lengths in the Linkages B_{12}–B_{12}, B_{22}–B_{22}, and B_{12}–B_{22}							
B(1)–B(12)	1.747(2)	B(10)–B(10)	1.630(3)	B(6)–B(14)	1.703(3)	B(9)–B(17)	1.706(3)
B(2)–B(2)	1.883(4)	B(13)–B(21)	1.716(3)	B(7)–B(15)	1.783(3)	B(23)–B(5)	1.906(3)
B(3)–B(11)	1.737(2)	B(4)–B(16)	1.671(3)	B(8)–B(20)	1.873(3)		
Sc–B, Sc–Si, Si–B, and Sc–Sc Distances							
Sc(1)–B(5)	2.298(2)	Sc(2)–B(24)	1.275(4)	Sc(3)–B(22)	2.231(3)	Si–B(13)	1.791(3)
–B(7)	2.386(2)	–B(14)	2.035(3)	–B(18)	2.309(4)	–B(23)	1.852(3)
–B(8)	2.387(2)	–B(15)	2.138(3)	–B(2)	2.327(3)	–B(24)	1.889(4)
–B(15)	2.406(2)	–B(18)	2.267(4)	–B(17)	2.349(3)	Sc(1)–Sc(3)	2.395(3)
–B(19)	2.419(2)	–B(20)	2.390(3)	–B(15)	2.364(3)	–Sc(2)	2.617(2)
–B(20)	2.427(2)	–B(23)	2.475(2)	–B(2)	2.384(3)	Sc(3)–Sc(3)	2.470(5)
–B(3)	2.458(2)	–B(8)	2.513(3)	–B(9)	2.445(3)		
–B(11)	2.462(2)	–B(7)	2.545(3)	–B(5)	2.488(3)		
–B(1)	2.463(2)	–B(6)	2.582(3)	Sc(2)–Si	1.422(3)		
–B(23)	2.476(1)	–B(13)	2.584(3)	Sc(3)–Si	1.723(3)		
–B(12)	2.480(2)	Sc(3)–B(24)	2.185(4)	Si–B(18)	1.030(4)		

simultaneous occupation can hardly occur. Thus, it is quite reasonable that the summation of the site occupancies of both sites is nearly 100%. The Al(3) and Al(5) sites in α-AlB_{12} are probably too narrow to accommodate Sc ions.

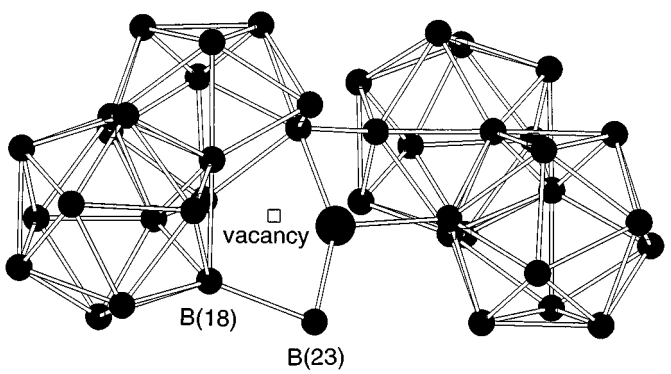

FIG. 4. The nature of the linkages between Si atoms and B_{22} units as seen along the *c*-axis where large and small circles correspond to Si and B atoms, respectively. One B(18) site in the left B_{22} unit must be empty because the site is too close to the Si site and is shown as a vacancy.

The Si–B lengths range from 1.791(3) to 1.889(4) Å with the average value of 1.844 Å in contrast to the Si–B bond lengths observed in SiB_6 where most of the Si–B bond lengths exceed 2.0 Å (16). These values come within the variational range of the B–B bond lengths. Thus, Si in the bridge site of $ScB_{19+x}Si_y$ plays an important role in tightly bonding two B_{22} units.

4. CONCLUDING REMARKS

The single crystals of $ScB_{19+x}Si_y$ which is isostructural with ScB_{19} could be successfully grown by the floating zone method, which proved that the Si addition method can be used widely in the melt growth of boron-rich borides. Structure analysis confirmed that $ScB_{19+x}Si_y$ and ScB_{19} are isotypic to α-AlB_{12} as expected in the previous paper.

Now there remains one question, whether $ScB_{19+x}Si_y$ can replace to YB_{66} as a new soft X-ray monochromator material. $ScB_{19+x}Si_y$ seems to satisfy most of material requirements, for example, a large *d*-spacing, vacuum compatibility, resistance to radiation damage, and so on. One important factor, i.e., thermal conductivity, has not been measured yet. Since the crystal structure of $ScB_{19+x}Si_y$ includes fewer atom sites with partial occupancy than YB_{66}, we may be able to expect a higher thermal conductivity than YB_{66}.

Another important factor is crystal quality. Can we achieve high crystal quality for $ScB_{19+x}Si_y$ crystals at a level sufficient for use in the monochromator? Actually we are not so optimistic about this. In the case of YB_{66} crystal growth even the first crystal growth trial achieved not only a single-grain crystal but also a rather narrow rocking curve width. On the other hand, it seems to be not so easy to obtain a crack-free and single-grain crystal of $ScB_{19+x}Si_y$ because the crystal growth mode is more like solution growth than melt growth as mentioned above. However, if we can get a crack-free and single-grain crystal, we could expect a high crystal quality because in general the solution growth gives a narrower rocking curve width than the melt growth. Further crystal growth efforts will be continued.

ACKNOWLEDGMENTS

The authors thank Mr. S. Takenouchi of this institute for performing the chemical analysis. They also thank Dr. I. Higashi of Chiba Institute of Technology for useful discussions on crystal structure analysis.

REFERENCES

1. M. Rowen *et al*., *Synchrotron Radiation News* **6**(3), 25 (1993).
2. T. Tanaka, S. Okada, Y. Yu, and Y. Ishizawa, *J. Solid State Chem.* **133,** 31 (1997).
3. T. Tanaka, S. Okada, and Y. Ishizawa, *J. Alloys Compd.* **205,** 281 (1994).
4. T. Tanaka, S. Okada, and V. N. Gurin, *J. Alloys Compd.* **267,** 211 (1998).
5. T. Tanaka, *J. Alloys Compd.* **270,** 132 (1998).
6. Y. Shi, A. Leithe-Jasper, and T. Tanaka, *J. Solid State Chem.* **148,** 250 (1999).
7. T. Tanaka, S. Okada, and Y. Ishizawa, *J. Solid State Chem.* **133,** 55 (1997).
8. I. Higashi, T. Tanaka, K. Kobayashi, Y. Ishizawa, and M. Takami, *J. Solid State Chem.* **133,** 31 (1997).
9. I. Higashi, T. Sakurai, and T. Atoda, *J. Solid State Chem.* **20,** 67 (1977); J. S. Kasper, M. Vlasse, and R. Naslain, *J. Solid State Chem.* **20,** 281 (1977).
10. K. E. Spear, "Phase Diagrams, Vol. IV," p. 91. Academic Press, San Diego, 1976.
11. A. Altomare, G. Cascarano, C. Giacovazzo, A. Guagliardi, M. C. Burla, G. Polidori, and M. Camalli, *J. Appl. Crystallogr.* **27,** 435 (1994).
12. G. M. Sheldrick, SHELX97: a program for the solution and refinement of crystal structures, Universität Göttingen, Göttingen, Germany, 1997.
13. M. Vlasse, R. Naslain, J. S. Kasper, and K. Ploog, *J. Less-Common Met.* **67,** 1 (1979).
14. I. Higashi, *J. Solid State Chem.* **154,** 168 (2000).
15. G. Will, *Acta Crystallogr.* **23,** 1071 (1967).
16. M. Vlasse, G. A. Slack, M. Garbauskas, J. S. Kasper, and J. C. Viala, *J. Solid State Chem.* **63,** 31 (1986).